JOC The Journal of Organic Chemistry

pubs.acs.org/joc Article

How Robust Is the Reversible Steric Shielding Strategy for Photoswitchable Organocatalysts?

Simone Gallarati,[‖] Raimon Fabregat,[‖] Veronika Juraskova, Theo Jaffrelot Inizan, and Clemence Corminboeuf*

Cite This: J. Org. Chem. 2022, 87, 8849−8857 Read Online

ACCESS | Metrics & More | Article Recommendations | Supporting Information

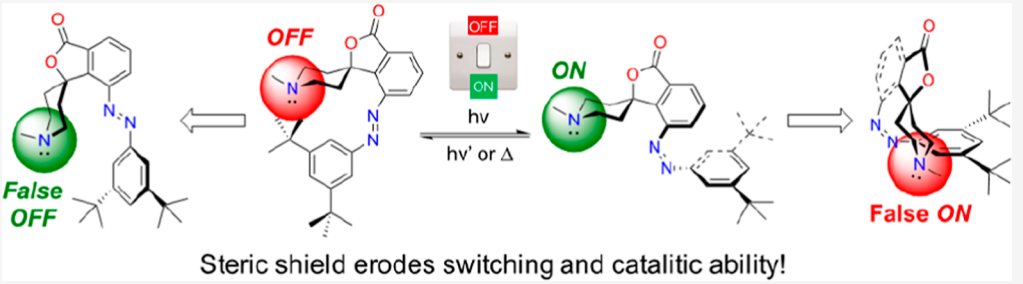

ABSTRACT: A highly appealing strategy to modulate a catalyst's activity and/or selectivity in a dynamic and noninvasive way is to incorporate a photoresponsive unit into a catalytically competent molecule. However, the description of the photoinduced conformational or structural changes that alter the catalyst's intrinsic reactivity is often reduced to a handful of intuitive static representations, which can struggle to capture the complexity of flexible organocatalysts. Here, we show how a comprehensive exploration of the free energy landscape of N-alkylated azobenzene-tethered piperidine catalysts is essential to unravel the conformational characteristics of each configurational state and explain the experimentally observed reactivity trends. Mapping the catalysts' conformational space highlights the existence of false ON or OFF states that lower their switching ability. Our findings expose the challenges associated with the realization of a reversible steric shielding for the photocontrol of Brønsted basicity of piperidine photoswitchable organocatalysts.

INTRODUCTION

Inspired by the regulation of the activity of enzymes through trigger-induced effects,[1] chemists are seeking to develop synthetic catalysts whose reactivity or principle of asymmetric induction can be modulated by external stimuli, such as temperature, pressure, or pH.[2] Light is another particularly attractive stimulus due to its noninvasiveness, high spatial and temporal resolution, and possibility of being manipulated precisely with modern optics.[3] In photoswitchable organocatalysis, electromagnetic irradiation induces a reversible transformation of a photochromic moiety incorporated into an organocatalytic system (*e.g.*, (*E*) → (*Z*) isomerization of a double bond).[4] The photochrome must be carefully chosen to ensure that the photoinduced reaction occurs with a high efficiency in both the forward and reverse directions, meaning high concentrations of either configuration can be obtained. This transformation must then cause a significant alteration of the steric or electronic properties of the catalyst, which leads to the two states having intrinsically different reactivities.[5] The configurational state displaying a higher reactivity is termed the ON state, while the one with a lower reactivity is called the OFF state.

Different strategies have been developed to attain this modulation of chemical reactivity with light, including activation,[6] inhibition,[7] templation,[8−19] electronic alteration,[20−28] and reversible steric shielding. The latter is a classic, conceptually elegant and, in principle, straightforward design strategy, exploited as early as 1981,[29,30] whereby access to either the substrate-binding site, or the catalytically active site, is restricted by a blocking group in the OFF state (Scheme 1). In the ON state, the photoinduced transformation/isomerization allows the blocking group to be moved away from the active site and the molecule to become catalytically active.[31] In an ideal scenario, there should be a one-to-one correspondence between a catalyst's configurational state (*e.g.*, (*E*)- or (*Z*)-isomer) and it being in either the ON or OFF state (*i.e.*, active-site shielded or deshielded), meaning that whenever the catalyst is, for example, in the (*Z*)-configuration, it is also in the

Received: December 8, 2021
Published: June 28, 2022

https://doi.org/10.1021/acs.joc.1c02991
J. Org. Chem. 2022, 87, 8849−8857

Scheme 1. Photoswitchable Azobenzene-Based Piperidine Organocatalysts for the Henry Reaction Exploiting Reversible Steric Shielding[a]

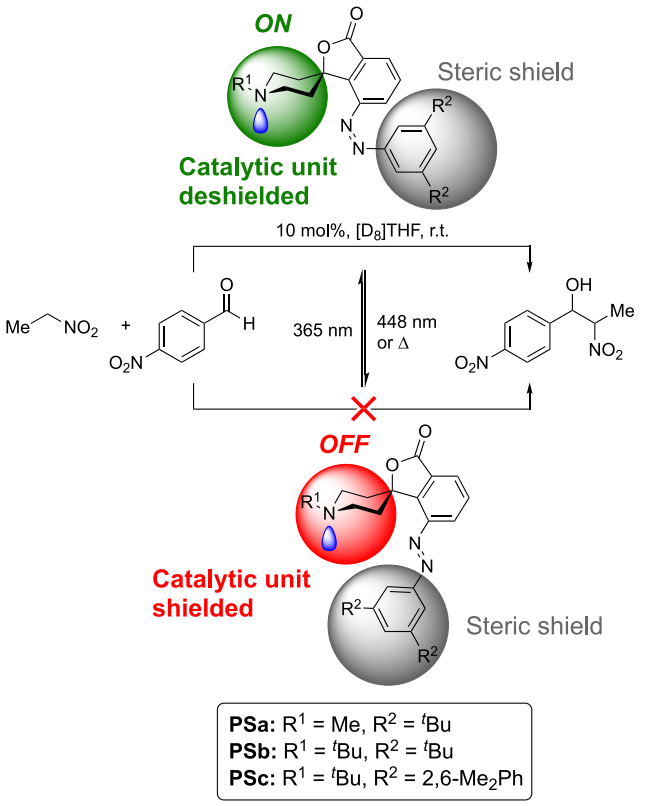

[a]In the (*E*)-configuration, a steric shield blocks access to the active site. In the (*Z*)-configuration, photoinduced switching frees access to the active site. This strategy relies on a one-to-one correspondence between the configuration and the ON/OFF state.

ON state (while the (*E*)-configuration is always OFF). Unfortunately, the conformational behavior of a photoswitchable organocatalyst can complicate this picture and break this correspondence down: since organocatalysts are generally rather flexible molecules with many low-energy, thermally accessible conformations, the same configuration might display both ON and OFF activity.

To understand the catalytic behavior of flexible organocatalysts that have been rationally designed based on reversible steric shielding (but also on hydrogen bonding templates, π-stacking, anion-π interactions, *etc.*),[32−36] the vast conformational space associated with their rich morphology must be thoroughly explored. Although conformational analysis is a familiar topic to organic chemists,[37] computational studies on organic systems are frequently limited to static density functional theory (DFT) depictions of isolated minima, aligning with textbook two-dimensional presentations of reaction mechanisms. This approach can fail, sometimes even leading to erroneous conclusions,[38] when medium-sized or large, highly flexible molecules that evolve on complex free energy surfaces (FES) are investigated.[39−43] While the conformational sampling of medium-sized organic systems can be performed with tools such as CREST,[44,45] the latter aims at improving the description of ensemble averages through Boltzmann reweighting of the optimized structures rather than at providing access to the free energy landscape. Ab initio molecular dynamics is limited to short time intervals ($\sim 10^2$ to 10^3 ps) in which chemically relevant interconversions between important states might not be explored.[46−49] Using potentials derived from semiempirical methods, such as density functional tight binding (DFTB)[50−56] or machine-learned potentials[57−63] that can reach the accuracy of quantum mechanical computations at a fraction of their computational cost, allows the simulation times to be lengthened, yet owing to the complexity of the free energy landscape of photoswitchable organocatalysts, visiting all possible conformational/configurational regions might still be impossible. Recently, our group exploited enhanced sampling techniques, combined with low-cost electronic structure computations[64] or neural network[65] and kernel-based potentials,[66] to address organic chemistry problems connected to fluxional molecules, such as organocatalysts[67,68] and molecular rotors.[69] Within this context, Hamiltonian or temperature replica exchange molecular dynamics (REMD)[70] are well-suited sampling approaches because they do not require any a priori knowledge of the dominant conformational regions or of the relevant collective variables characterizing them and are able to generate unbiased canonical sampling at a particular temperature.[66]

In this work, we use parallel tempering REMD simulations at the DFTB3 level[71−73] to investigate the FES and the corresponding configurational and conformational behavior of an early example of photoreversible steric shielding, namely the azobenzene-tethered N-alkylated piperidine base catalysts developed by Hecht and co-workers (Scheme 1).[74−77] This elegantly designed system consists of a piperidine Brønsted base and a photochromic azobenzene moiety that are rigidly and orthogonally positioned through the spiro junction of an isobenzofuranone ring. In the thermodynamically more stable (*E*)-isomer, the 3,5-substituents on the phenylazo unit shields the basic site; UV irradiation affords the metastable (*Z*)-isomer and exposes the nitrogen lone pair, enhancing the basicity by almost one order of magnitude and the rate of the Henry reaction[78,79] between nitroethane and *p*-nitrobenzaldehyde. Analysis of the potential energy surface of **PSa−c**, obtained through the computation of a handful of static DFT geometries, in combination with NMR experiments, was previously used to optimize the catalyst's structure.[75] However, this approach cannot fully explain the observed reactivity trends of photoswitches **PSa−c** (Scheme 1). Our simulations shed light on the subtle interplay between conformational states and activity and expose the possible drawbacks of reversible steric shielding as a design strategy to achieve light-gated modulation of chemical reactivity.

COMPUTATIONAL DETAILS

All potential energy computations were performed in the gas phase at the DFTB3/3OB[72,73] level in combination with the D3BJ[80] dispersion correction, as implemented in DFTB+ software.[81] DFTB is two to three orders of magnitude faster than *ab initio* and DFT methods, making it particularly attractive in applications to large molecules and condensed phase systems, especially when extensive sampling is important to the reactive process of interest. Static DFT and DFTB3 computations were performed with Gaussian16[82] and AMS2020.1[83,84] software packages to assess the impact of the level of theory on the barrier heights and relative stability of different conformations. Parallel tempering (PT) replica exchange simulations were performed using the REMD@DFTB3[64] protocol implemented in i-PI[85] to sample the

https://doi.org/10.1021/acs.joc.1c02991
J. Org. Chem. 2022, 87, 8849−8857

Scheme 2. Schematic Representation of Local Minima and Transition States Rationalized according to Chemical Intuition and Static DFT Computations[75a]

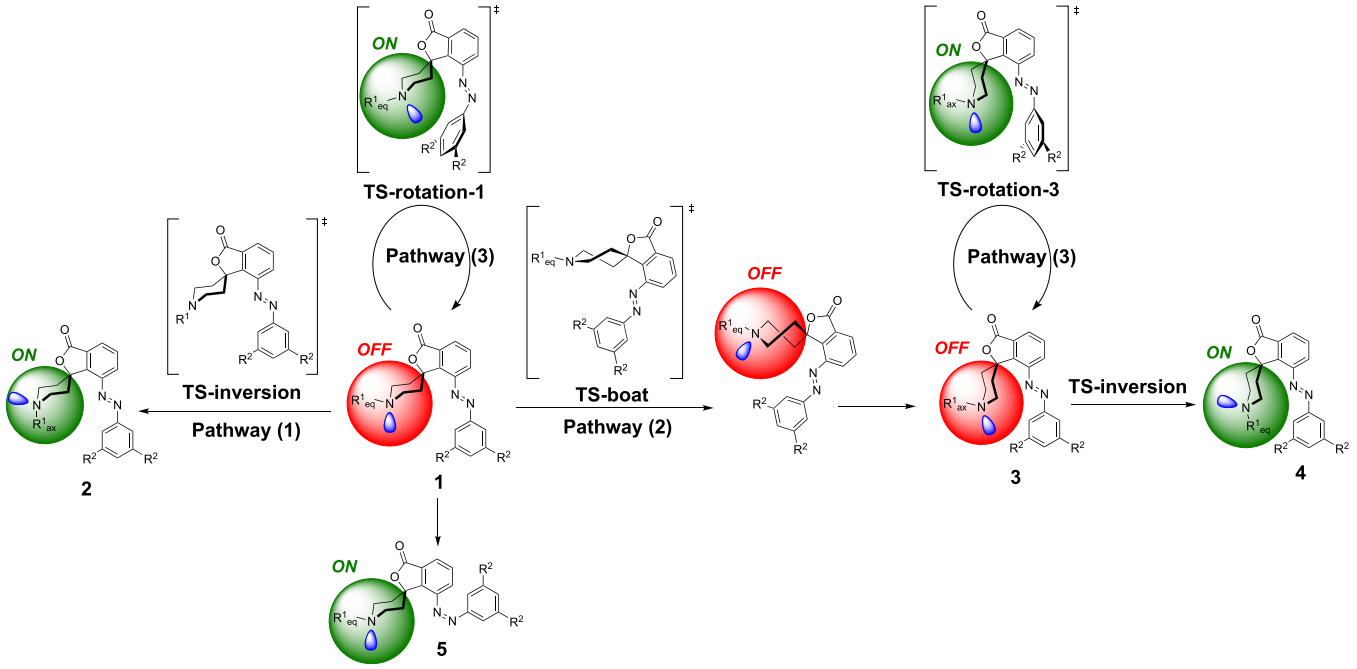

[a]Reproduced from Stoll, R. S.; Peters, M. V.; Kuhn, A.; Heiles, S.; Goddard, R.; Bühl, M.; Thiele, C. M.; Hecht, S. J. Am. Chem. Soc. 2009, 131 (1), 357−367. Copyright 2009 American Chemical Society.

canonical (*i.e.*, *NVT*) ensemble at the target temperature of 300 K for each photoswitchable organocatalyst. In PT-REMD, a series of energetically independent trajectories (called replicas) of the same system at different temperatures is simulated, allowing complete configurations from replicas at these temperatures to be occasionally exchanged. The exchange between replicas propagated at higher temperatures, where energy barriers can be overcome and a large amount of the FES is explored, and those at a lower temperature, constrained to local minima of the FES, ensures converged statistical sampling at a target temperature and thorough exploration of the free energy landscape. The (*E*)- and (*Z*)-configurations of each species were sampled in independent simulations, using a harmonic restraint to maintain the organocatalyst in a specific configuration throughout the simulation. The restraint was introduced in the dynamics using PLUMED[86−88] software. The simulations included 16 replicas with temperatures ranging from 300 to 1200 K separated by logarithmic intervals. A time step of 0.6 fs was used in the dynamics, with a Langevin thermostat to control the temperature. To ensure the convergence of the sampling, we ran the simulations for 1.2 ns and analyzed the evolution of the integrated free energy differences between basins at 300 K. As the crossing of energy barriers is associated with the slowest dynamic modes of the systems, their convergence is a reliable estimation of the overall convergence of the sampling (see the Supporting Information). The interactive plots were constructed with Python framework Dash for web applications (https://plotly.com/dash/).

While it is well-known that dispersion-corrected DFTB3/3OB leads to potentials significantly flatter[64,66,72,89,90] than those computed with a higher electronic structure level, the consequences of these shortcomings have been extensively discussed.[64,66,72,90] The reader is thus pointed to refs 64, 66, 72, 89, and 90 for further technical considerations on the topic. Importantly, it has been demonstrated by us and others that the low-cost computational level provides a reliable description of organic chemical reactions[90] and is capable of identifying all the relevant conformational regions accessible around 300 K. For the photoswitchable systems investigated herein, differences between static scans of selected collective variables at the DFTB3 and DFT levels (*i.e.*, without conformational entropy corrections) and comparisons with the FESs (accounting for conformational entropy) are discussed in the Supporting Information. In addition, the consequence of the relative flatness of the low-cost potential on the relative population of catalytically active or inactive states by **PSa−c** is discussed. Overall, it is confirmed that accounting for the full conformational entropy and anharmonic effects is more transformative for the relative population of the conformational regions than the use of higher-level potentials.

RESULTS AND DISCUSSION

Analysis of the Free-Energy Maps. The conformational analysis of **PSa−c** has previously[75] been reduced to the limited number of chemically intuitive static representations **1−5** shown in Scheme 2, and three pathways have been considered to account for the catalysts' residual activity in the (*E*)-state: (1) inversion of the piperidine N-atom; (2) inversion of the piperidine chair, that is, "ring flip", leading to the more stable conformer **4** after N-inversion; (3) rotation of the blocking group around the (N═N)−Ph bond, placing the benzofuranone and phenylazo groups in an orthogonal orientation and allowing the substrate to be deprotonated by piperidine in its most stable chair conformation with the R^1 group in the equatorial position. Similar processes (N-inversion, ring flip, and rotation) can also occur in the (*Z*)-configuration but are expected to be less impactful on the catalytic activity as the N-

https://doi.org/10.1021/acs.joc.1c02991
J. Org. Chem. 2022, 87, 8849−8857

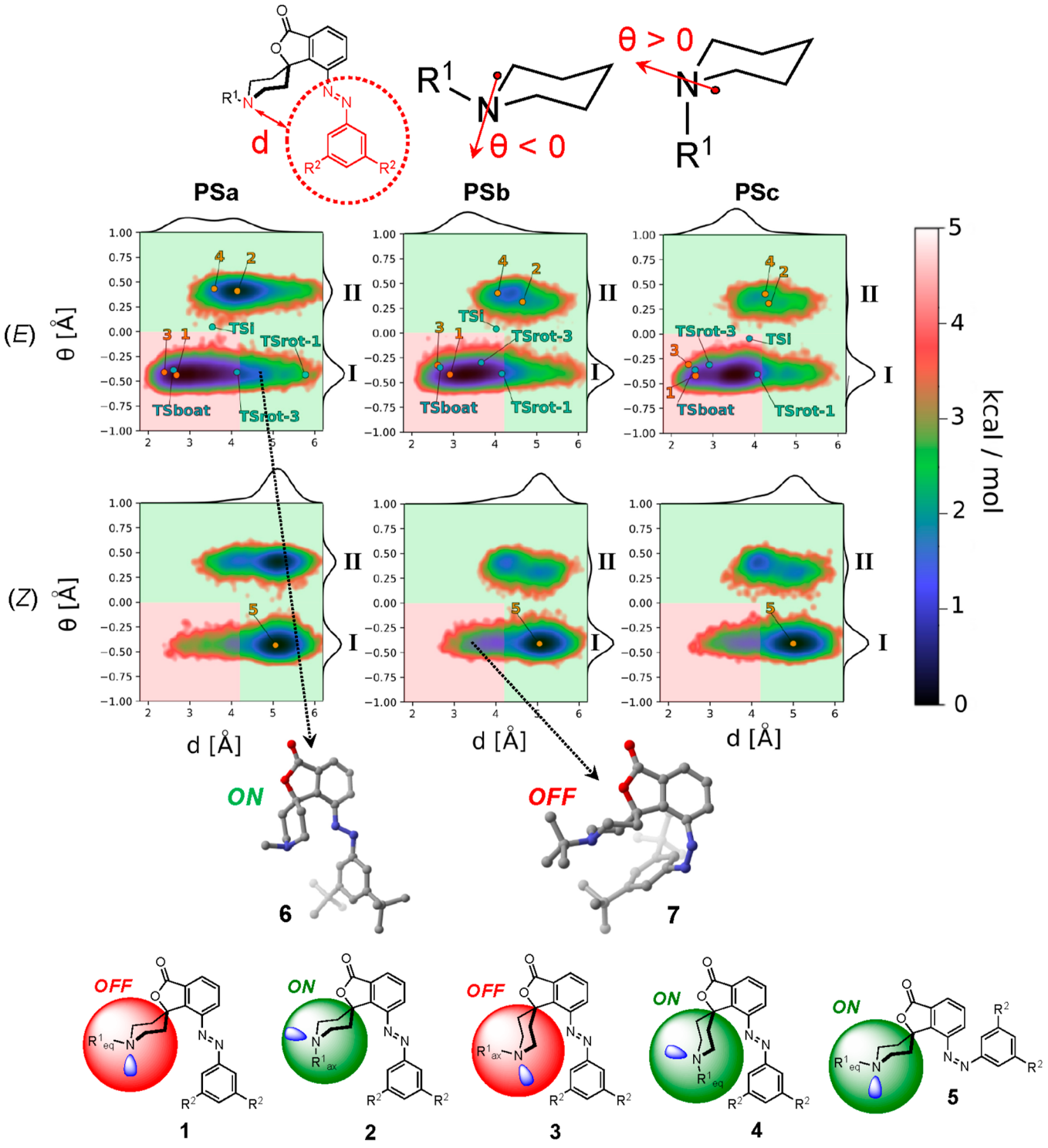

Figure 1. Two-dimensional representation of the free energy landscape corresponding to the *NVT* ensemble at 300 K obtained from the REMD@DFTB3 of (*E*)- (top) and (*Z*)-**PSa−c** (bottom). The relevant collective variables are shown at the top. The regions of the landscapes are colored in green or red according to the ON or OFF function of the photoswitches. The orange and blue points represent the local minima and transition states (labeled according to Scheme 2) optimized at the DFTB3 level from the static geometries reported in ref 75. Distribution histograms according to d and θ are shown on the top and right axes of the plots, respectively.

lone pair should always remain accessible. On the other hand, a finite temperature exploration of a molecule's free energy landscape (Figure 1) may alter, if not even reverse, pictures provided by static relative energy computations.[64]

Figure 1 shows the 2D FES corresponding to the *NVT* ensemble at 300 K of **PSa−c** represented in terms of two collective variables, d and θ. The former is the shortest distance between the nitrogen atom of the piperidine ring and any other atom of the phenylazo group. The latter is the distance between the piperidine's N-atom and the plane passing through the three carbon atoms the nitrogen is bound to (R^1-C and two C-atoms of the piperidine ring). If the nitrogen

https://doi.org/10.1021/acs.joc.1c02991
J. Org. Chem. 2022, 87, 8849−8857

is located below this plane, θ adopts negative values; if N is above the plane, θ is positive (see Figure 1). The conformational region with $\theta < 0$ is labeled **I**, and the one with $\theta > 0$ is labeled **II**. Each FES is divided into two areas, colored green or red, according to the values of d and θ. The red area indicates that the catalyst's basic site (*i.e.*, the nitrogen's lone pair) is sterically shielded, while the green one indicates that it is deshielded.[91] Interactive plots showing the conformational states used to construct the FES are freely available as a Heroku deployed app (https://photoswitch-exp.herokuapp.com/).

In the (*E*)-state plots, region **I** is the conformational region associated with **1** and **3** and the transition states for ring flip and rotation; region **II** contains **2** and **4**, while transitions between the two regions are associated with the inversion transition state (Scheme 2). For comparison with the static picture, the structures previously determined with DFT computations,[75] reoptimized at the DFTB3 level, are included as the orange and blue points in Figure 1.

Region **I** of (*E*)-**PSa** has the largest conformational entropic contributions, as indicated by the larger basin and small REMD free energy differences between the ring-flipped conformers (the DFTB3 free energy difference between the red and green areas of basin **I** of (*E*)-**PSa** is 1.3 kcal/mol, *vs* 2.1 kcal/mol for (*E*)-**PSc**). Since there are many possible twist or twist-boat intermediates and transition states, depending on which C−C or C−N bond of the piperidine ring is rotated relative to its opposite counterpart and in what direction, the generation of ring-flipped conformers cannot be thought of as an individual process but rather as the population of a continuum of twist-boat (or twist) conformational states, which cannot easily be captured by a static minimum-energy structure search approach. Compared to (*E*)-**PSb**−**c**, the broader conformational region **I** of (*E*)-**PSa** is associated with the population of false OFF states in which the benzofuranone and phenylazo rings are oriented orthogonally to each other through rotation around the (N═N)−Ph bond (see, *e.g.*, **6** on the bottom left corner of Figure 1). In (*E*)-**PSb** and **PSc**, the bulkier R^2 groups (^{t}Bu or 2,6-Me_2Ph) help more effectively shield the lone pair, making region **I** more structured in the red area of the plot.

The small energy difference between region **I** and **II** of (*E*)-**PSa** (0.5 kcal/mol) suggests that N-inverted species with the R^1 (Me) group in the axial position and rearranged conformers with equatorial R^1 and exposed N-lone pairs are significantly populated. Experimentally, the ^{13}C NMR shift of the *N*-methyl carbon of (*E*)-**PSa** was found to lie in between the shifts for axial and equatorial positions.[75] This suggests that N-inversion is fast on the NMR timescale, in agreement with the significant population of region **II** and fast exchange of the *N*-methyl between axial and equatorial positions. In **PSb** and **PSc**, basin **II** is smaller and possesses higher relative free energies (1.2 and 1.7 kcal/mol, respectively), indicating that N-inversion in these catalysts is suppressed. This relates well with the larger size of the R^1 substituent (^{t}Bu group) and its unlikeliness of adopting the axial position in a six-membered ring.

The conformational space in the (*Z*)-configuration is narrower (the FES possesses a more distinct minimum) than in the (*E*)-state (the FES is flatter). The minimum of region **I** of (*Z*)-**PSa** is clearly located within the green area of the plot. Owing to the small ratio between the van der Waals volumes of R^1 (Me, 25.8 Å^3) and R^2 (^{t}Bu, 72 Å^3),[92] only a small fraction of false ON states in which the active site is shielded is populated. Like in the (*E*)-state, regions **I** and **II** of (*Z*)-**PSa** possess similar free energies and an inversion at the piperidine's N-atom with an exchange of the axial lone pair and equatorial methyl group has a high probability of occurring. Region **II** of (*Z*)-**PSb**−**c** is less frequently visited due to the unlikeness of inverting the bulkier R^1 (^{t}Bu) group, which would lead to significantly unfavorable 1,3-diaxial interactions. On the other hand, (*Z*)-**PSb** and (*Z*)-**PSc** have a higher probability than (*Z*)-**PSa** of visiting the red area of the plot; despite having the same R^2 group as **PSa** (^{t}Bu), **PSb** is more likely to populate false ON states in which the blocking group shields the catalytically active site due to a rotation of the benzofuranone−azo bond (*e.g.*, structure **7** on the bottom right corner of Figure 1). Although the *meta*-xylene R^2 group of **PSc** (110.6 Å^3) is bigger than *tert*-butyl in **PSb** (72 Å^3),[93] the aromatic ring is "flatter" than the alkyl substituent and, therefore, less likely to shield the basic site in the (*Z*)-configuration. Thus, **PSc** has a lower probability than **PSb** to populate false ON states.

Overall, an inspection of the Figure 1 plots shows that none of the catalysts examined is ideally tuned for reversible steric shielding: in an ideal photoswitchable catalyst, the conformational space of each configuration should be totally restricted to either the red or green area. However, within each (*E*)- or (*Z*)-plot, basins located both in the green and red areas are populated. The broad conformational space of (*E*)-**PSa** and (*Z*)-**PSb**−**c** is illustrative of the importance of capturing the full anharmonic and entropic contributions to the free energy landscape: computing a "static" population of few representative conformers cannot properly account for the existence of false OFF and false ON states that reduce the catalysts' switching ability.

Relating Conformational Behavior with Experimental Reactivity. Kinetic studies on the catalytic performance of the three photoswitchable catalysts showed that, in the (*E*)-configuration, **PSa** is the most active, while **PSc** leads to an essentially trace yield of β-nitro alcohol (Table 1).[75] This is consistent with the free energy maps in Figure 1, which show that the ^{t}Bu group of **PSc**−**b** serves as an efficient conformational anchor for the six-membered piperidine ring

Table 1. Photochemical, Kinetic, and Thermodynamic Experimental Data of Piperidine Bases PSa−c Taken from Ref 75[a]

	PSa	PSb	PSc
PSS (*Z*/*E*)[b]	90:10	90:10	>90:10
$t_{1/2}$[c] [h]	268	286	466
k_E[d] [10^{-6} s^{-1}]	5.0	0.96	0.39
Y_E[e] (%)	25	6	0
k_Z[f] [10^{-6} s^{-1}]	22.0	13.0	14.0
Y_Z[g] (%)	72	47	57
k_{rel} (k_Z/k_E)	4.4	13.5	35.9
ΔpK_a[h]		0.8	0.7

[a]Reproduced from Stoll, R. S.; Peters, M. V.; Kuhn, A.; Heiles, S.; Goddard, R.; Bühl, M.; Thiele, C. M.; Hecht, S. J. Am. Chem. Soc. 2009, 131 (1), 357−367. Copyright 2009 American Chemical Society. [b]Photostationary state (PSS) obtained by irradiation at 365 nm. [c]Half-life of the (*Z*)-isomer at 20 °C. [d]Rate constant of the Henry reaction using pul(*E*)-isomer. [e]2-Nitro-1-(4-nitrophenyl)propan-1-ol yield usingIre (*E*)-isomer. [f]Rate constant of the Henry reaction extrapolated to 100% (*Z*)-isomer. [g]2-Nitro-1-(4-nitrophenyl)propan-1-ol yield extrapolated to 100% (*Z*)-isomer. [h]Difference of pK_a values, *i.e.*, pK_a(PSS) − pK_a(*E*), obtained from titration with triflic acid using neutral red as a reference base.

https://doi.org/10.1021/acs.joc.1c02991
J. Org. Chem. 2022, 87, 8849−8857

and that the *meta*-xylene R^2 group improves the efficiency of blocking the active site, localizing the minimum of the FES of (*E*)-**PSc** in the red inactive region. On the other hand, (*E*)-**PSa** can access enthalpically and entropically favored conformational states in the green active region due to inversion at the piperidine's N-atom and rotation around the (N═N)−Ph bond.

The free energy plots of the (*Z*)-configuration suggest that **PSa** has a lower probability than **PSb** or **PSc** of visiting the red area of the FES thanks to the small size ratio of its R^1 and R^2 groups and their inability to effectively shield the lone pair. Consistently, (*Z*)-**PSa** displays the highest rate and yield in the Henry reaction (Table 1). Owing to region **I** of their FES being broader, along with the higher energy difference between basin **I** and **II**, (*Z*)-**PSb** and (*Z*)-**PSc** can access inactive states through rotation around the isobenzofuranone core and thus have a lower catalytic activity.

The switching ability of catalysts **PSa**−**c** can also be rationalized according to the conceptual plot shown in Figure 2, where the relative rate (k_Z/k_E) is expressed as a function of

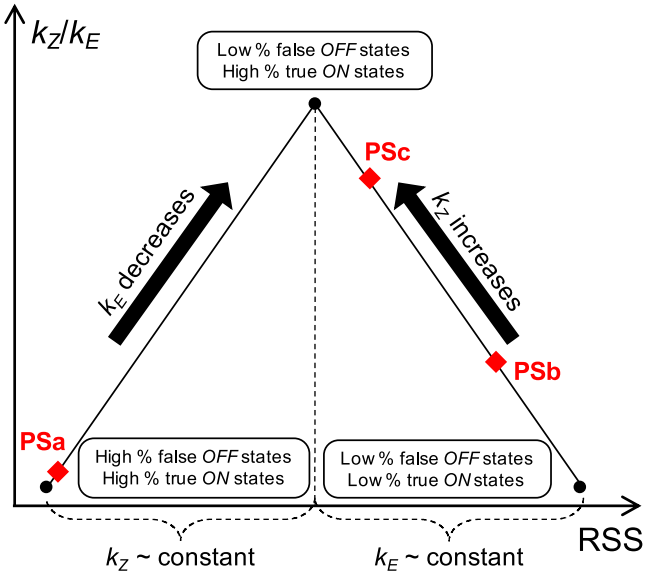

Figure 2. Conceptual plot showing the correlation between the conformational behavior of photoswitches **PSa**−**c** and their switching ability (k_{rel} *i.e.*, k_Z/k_E). RSS is a hypothetical reversible steric shielding descriptor.

the conformational behavior. At the top of this plot lies the ideal photoswitchable organocatalyst, whose distribution of conformations in the (*E*)-state is always inactive, while in the (*Z*)-state is always active. This would correspond to an ideal free energy map in which the conformational space of each configuration is totally restricted to either the red or green area. At the bottom of the left and right sides lie the "worst" catalysts, namely those in which false OFF states are significantly populated (left side) or true ON states are scarcely populated (right side). On traversing the plot left to right, populating false OFF states becomes increasingly more difficult due to a more structured (*E*)-state and k_E decreases, while the population of true ON states (*i.e.*, k_Z) is assumed to remain approximately constant until the peak is reached. Further progression to the right corresponds to a reduction of k_Z (with k_E ca. the same) since the (*Z*)-configuration becomes more flexible, leading to false ON states being populated.

PSa lies toward the bottom of the left side of the plot due to its highly flexible (*E*)-configuration and significant population of N-inverted and (N═N)−Ph rotated conformers; **PSb** is located on the opposite side, because of the likeliness of populating (*Z*)-conformational states in which the phenylazo unit shields the piperidine's N-atom. Interestingly, **PSc**, although possessing the highest k_{rel} (Table 1), is not located at the top of the plot because, compared to **PSa**, it has a less structured (*Z*)-state, and true ON states are populated to a lesser extent, implying the possibility of further improvement. Reversible steric shielding is clearly a double-edged sword: while the introduction of the large *tert*-butyl group on the piperidine ring and of the *meta*-xylene substituent on the phenylazo unit effectively maximizes the population of true OFF states in the (*E*)-configuration, locking the piperidine ring with an axial lone pair adequately shielded by the R^2 substituent, it simultaneously leads to a less structured (*Z*)-configuration in which false ON states are more frequently visited.

Although the present analysis was performed in the gas phase (the inclusion of an explicit solvent is not easily compatible with PT)[94] and at a fairly low electronic structure level (REMD@DFTB3), the key findings related to the conformational behavior of the photoswitchable catalysts examined remain valid. In particular, solvent effects tend to flatten the DFT (or higher)-based FES (see Table S2).[66] Overall, the relative population of catalytically active or inactive states of **PSa**−**c**, corroborated by comparison to the experimentally observed reactivity trends, is not expected to significantly change. While obtaining both highly accurate energetics and converged statistical sampling has typically hampered the appropriate description of the flexibility of organic molecules, efforts in our group are being made to achieve *ab initio* accuracy by correcting semiempirical potentials with machine learning models, including implicit[66] or explicit treatment of solvation.[65,95]

CONCLUSIONS

In this work, we have illustrated the importance of thoroughly exploring of the free energy landscape of flexible photoswitchable organocatalysts to understand their catalytic performance. Without any *a priori* knowledge of the system, the complex FES of three N-alkylated azobenzene-tethered piperidine photoswitches were successfully mapped, the energetic basins corresponding to the structural minima identified, and the experimentally observed reactivity trends rationalized according to the catalysts' conformational behavior. Our findings show that the lack of highly structured configurations and the access to entropically favored regions in one state can limit the effectiveness of reversible steric shielding as a design strategy to attain photoregulation of chemical reactivity. While large substituents and steric clashes may have a beneficial effect in one configuration, leading to a limited number of false OFF states being populated, they can simultaneously result in the population of false ON states in the other, eroding a catalyst's photoswitching ability. This example explicitly illustrates the difficulty of achieving structure-based optimization on the basis of a static picture. In this respect, free energy sampling appears necessary to predict the impact of the floppy or bulky nature of different substituents on the conformational landscape of the ON/OFF states in the search of improved azobenzene derivatives with a higher structural rigidity.

https://doi.org/10.1021/acs.joc.1c02991
J. Org. Chem. 2022, 87, 8849−8857

■ ASSOCIATED CONTENT

Supporting Information

The Supporting Information is available free of charge at https://pubs.acs.org/doi/10.1021/acs.joc.1c02991.

Computational details, alternative and supplementary free energy and potential energy plots, distribution histograms, and relations with experimental data (PDF)

■ AUTHOR INFORMATION

Corresponding Author

Clemence Corminboeuf − *Laboratory for Computational Molecular Design, Institute of Chemical Sciences and Engineering, Ecole Polytechnique Fédérale de Lausanne (EPFL), Lausanne 1015, Switzerland; National Center for Competence in Research—Catalysis (NCCR-Catalysis) and National Center for Computational Design and Discovery of Novel Materials (MARVEL), Ecole Polytechnique Fédérale de Lausanne (EPFL), Lausanne 1015, Switzerland;* orcid.org/0000-0001-7993-2879; Email: clemence.corminboeuf@epfl.ch

Authors

Simone Gallarati − *Laboratory for Computational Molecular Design, Institute of Chemical Sciences and Engineering, Ecole Polytechnique Fédérale de Lausanne (EPFL), Lausanne 1015, Switzerland*

Raimon Fabregat − *Laboratory for Computational Molecular Design, Institute of Chemical Sciences and Engineering, Ecole Polytechnique Fédérale de Lausanne (EPFL), Lausanne 1015, Switzerland*

Veronika Juraskova − *Laboratory for Computational Molecular Design, Institute of Chemical Sciences and Engineering, Ecole Polytechnique Fédérale de Lausanne (EPFL), Lausanne 1015, Switzerland*

Theo Jaffrelot Inizan − *Laboratory for Computational Molecular Design, Institute of Chemical Sciences and Engineering, Ecole Polytechnique Fédérale de Lausanne (EPFL), Lausanne 1015, Switzerland*

Complete contact information is available at: https://pubs.acs.org/10.1021/acs.joc.1c02991

Author Contributions

‖S.G. and R.F. contributed equally to this work.

Notes

The authors declare no competing financial interest.

■ ACKNOWLEDGMENTS

The authors are grateful to the EPFL for the financial support. S.G., R.F. and C.C. acknowledge funding from the European Research Council (ERC, grant agreement no. 817977) within the framework of European Union's H2020. V.J. and C.C. acknowledge funding from the Swiss National Science Foundation (SNSF, no. 200020_175496).

■ REFERENCES

(1) Lüning, U. Switchable Catalysis. *Angew. Chem., Int. Ed.* **2012**, *51*, 8163−8165.

(2) Vlatković, M.; Collins, B. S.; Feringa, B. L. Dynamic Responsive Systems for Catalytic Function. *Chem.—Eur. J.* **2016**, *22*, 17080−17111.

(3) Blanco, V.; Leigh, D. A.; Marcos, V. Artificial Switchable Catalysts. *Chem. Soc. Rev.* **2015**, *44*, 5341−5370.

(4) Dorel, R.; Feringa, B. L. Photoswitchable Catalysis Based on the Isomerisation of Double Bonds. *Chem. Commun.* **2019**, *55*, 6477−6486.

(5) Neilson, B. M.; Bielawski, C. W. Illuminating Photoswitchable Catalysis. *ACS Catal.* **2013**, *3*, 1874−1885.

(6) Sugimoto, H.; Kimura, T.; Inoue, S. Photoresponsive Molecular Switch to Control Chemical Fixation of CO_2. *J. Am. Chem. Soc.* **1999**, *121*, 2325−2326.

(7) Ueno, A.; Takahashi, K.; Osa, T. Photoregulation of Catalytic Activity of β-Cyclodextrin by an Azo Inhibitor. *J. Chem. Soc., Chem. Commun.* **1980**, *17*, 837−838.

(8) Würthner, F.; Rebek, J., Jr. Light-Switchable Catalysis in Synthetic Receptors. *Angew. Chem., Int. Ed. Engl.* **1995**, *34*, 446−448.

(9) Cacciapaglia, R.; Di Stefano, S.; Mandolini, L. The Bis-Barium Complex of a Butterfly Crown Ether as a Phototunable Supramolecular Catalyst. *J. Am. Chem. Soc.* **2003**, *125*, 2224−2227.

(10) Wang, J.; Feringa, B. L. Dynamic Control of Chiral Space in a Catalytic Asymmetric Reaction Using a Molecular Motor. *Science* **2011**, *331*, 1429.

(11) Pizzolato, S. F.; Collins, B. S. L.; van Leeuwen, T.; Feringa, B. L. Bifunctional Molecular Photoswitches Based on Overcrowded Alkenes for Dynamic Control of Catalytic Activity in Michael Addition Reactions. *Chem.—Eur. J.* **2017**, *23*, 6174−6184.

(12) Osorio-Planes, L.; Rodríguez-Escrich, C.; Pericàs, M. A. Photoswitchable Thioureas for the External Manipulation of Catalytic Activity. *Org. Lett.* **2014**, *16*, 1704−1707.

(13) De Bo, G.; Leigh, D. A.; McTernan, C. T.; Wang, S. A Complementary Pair of Enantioselective Switchable Organocatalysts. *Chem. Sci.* **2017**, *8*, 7077−7081.

(14) Zhao, D.; Neubauer, T. M.; Feringa, B. L. Dynamic Control of Chirality in Phosphine Ligands for Enantioselective Catalysis. *Nat. Commun.* **2015**, *6*, 6652.

(15) Vlatković, M.; Bernardi, L.; Otten, E.; Feringa, B. L. Dual Stereocontrol over the Henry Reaction Using a Light- and Heat-Triggered Organocatalyst. *Chem. Commun.* **2014**, *50*, 7773−7775.

(16) Vlatković, M.; Volarić, J.; Collins, B. S. L.; Bernardi, L.; Feringa, B. L. Dynamic Control over Catalytic Function Using Responsive Bisthiourea Catalysts. *Org. Biomol. Chem.* **2017**, *15*, 8285−8294.

(17) Pizzolato, S. F.; Štacko, P.; Kistemaker, J. C. M.; van Leeuwen, T.; Feringa, B. L. Phosphoramidite-Based Photoresponsive Ligands Displaying Multifold Transfer of Chirality in Dynamic Enantioselective Metal Catalysis. *Nat. Catal.* **2020**, *3*, 488−496.

(18) Arif, T.; Cazorla, C.; Bogliotti, N.; Saleh, N.; Blanchard, F.; Gandon, V.; Métivier, R.; Xie, J.; Voituriez, A.; Marinetti, A. Bimetallic Gold(I) Complexes of Photoswitchable Phosphines: Synthesis and Uses in Cooperative Catalysis. *Catal. Sci. Technol.* **2018**, *8*, 710−715.

(19) Kondo, M.; Nakamura, K.; Krishnan, C. G.; Takizawa, S.; Abe, T.; Sasai, H. Photoswitchable Chiral Phase Transfer Catalyst. *ACS Catal.* **2021**, *11*, 1863−1867.

(20) Kano, N.; Yoshino, J.; Kawashima, T. Photoswitching of the Lewis Acidity of a Catecholborane Bearing an Azo Group Based on the Change in Coordination Number of Boron. *Org. Lett.* **2005**, *7*, 3909−3911.

(21) Lemieux, V.; Spantulescu, M. D.; Baldridge, K. K.; Branda, N. R. Modulating the Lewis Acidity of Boron Using a Photoswitch. *Angew. Chem., Int. Ed.* **2008**, *47*, 5034−5037.

(22) Wilson, D.; Branda, N. R. Turning "On" and "Off" a Pyridoxal 5′-Phosphate Mimic Using Light. *Angew. Chem., Int. Ed.* **2012**, *51*, 5431−5434.

(23) Eisenreich, F.; Kathan, M.; Dallmann, A.; Ihrig, S. P.; Schwaar, T.; Schmidt, B. M.; Hecht, S. A Photoswitchable Catalyst System for Remote-Controlled (Co)Polymerization in Situ. *Nat. Catal.* **2018**, *1*, 516−522.

(24) Imahori, T.; Yamaguchi, R.; Kurihara, S. Azobenzene-Tethered Bis(Trityl Alcohol) as a Photoswitchable Cooperative Acid Catalyst for Morita-Baylis-Hillman Reactions. *Chem.—Eur. J.* **2012**, *18*, 10802−10807.

(25) Neilson, B. M.; Bielawski, C. W. Photoswitchable Organocatalysis: Using Light To Modulate the Catalytic Activities of N-Heterocyclic Carbenes. *J. Am. Chem. Soc.* **2012**, *134*, 12693−12699.
(26) Neilson, B. M.; Bielawski, C. W. Photoswitchable Metal-Mediated Catalysis: Remotely Tuned Alkene and Alkyne Hydroborations. *Organometallics* **2013**, *32*, 3121−3128.
(27) Weston, C. E.; Richardson, R. D.; Fuchter, M. J. Photoswitchable Basicity through the Use of Azoheteroarenes. *Chem. Commun.* **2016**, *52*, 4521−4524.
(28) Iida, H.; Umebayashi, N.; Yashima, E. Photoswitchable Organocatalysis in Acylation of Alcohol Using Dithienylethene-Linked Azoles. *Tetrahedron* **2013**, *69*, 11064−11069.
(29) Ueno, A.; Takahashi, K.; Osa, T. Photocontrol of Catalytic Activity of Capped Cyclodextrin. *J. Chem. Soc., Chem. Commun.* **1981**, *3*, 94−96.
(30) Lee, W.-S.; Ueno, A. Photocontrol of the Catalytic Activity of a β-Cyclodextrin Bearing Azobenzene and Histidine Moieties as a Pendant Group. *Macromol. Rapid Commun.* **2001**, *22*, 448−450.
(31) Stoll, R. S.; Hecht, S. Artificial Light-Gated Catalyst Systems. *Angew. Chem., Int. Ed.* **2010**, *49*, 5054−5075.
(32) Romanazzi, G.; Degennaro, L.; Mastrorilli, P.; Luisi, R. Chiral Switchable Catalysts for Dynamic Control of Enantioselectivity. *ACS Catal.* **2017**, *7*, 4100−4114.
(33) Göstl, R.; Senf, A.; Hecht, S. Remote-Controlling Chemical Reactions by Light: Towards Chemistry with High Spatio-Temporal Resolution. *Chem. Soc. Rev.* **2014**, *43*, 1982.
(34) Schaufelberger, F.; Ramström, O. Kinetic Self-Sorting of Dynamic Covalent Catalysts with Systemic Feedback Regulation. *J. Am. Chem. Soc.* **2016**, *138*, 7836−7839.
(35) Neel, A. J.; Hilton, M. J.; Sigman, M. S.; Toste, F. D. Exploiting Non-Covalent π Interactions for Catalyst Design. *Nature* **2017**, *543*, 637−646.
(36) Uyeda, C.; Jacobsen, E. N. Transition-State Charge Stabilization through Multiple Non-Covalent Interactions in the Guanidinium-Catalyzed Enantioselective Claisen Rearrangement. *J. Am. Chem. Soc.* **2011**, *133*, 5062−5075.
(37) Brethomé, A. V.; Fletcher, S. P.; Paton, R. S. Conformational Effects on Physical-Organic Descriptors: The Case of Sterimol Steric Parameters. *ACS Catal.* **2019**, *9*, 2313−2323.
(38) Plata, R. E.; Singleton, D. A. A Case Study of the Mechanism of Alcohol-Mediated Morita Baylis−Hillman Reactions. The Importance of Experimental Observations. *J. Am. Chem. Soc.* **2015**, *137*, 3811−3826.
(39) Allemann, C.; Gordillo, R.; Clemente, F. R.; Cheong, P. H.-Y.; Houk, K. N. Theory of Asymmetric Organocatalysis of Aldol and Related Reactions: Rationalizations and Predictions. *Acc. Chem. Res.* **2004**, *37*, 558−569.
(40) Kaczor, A.; Reva, I. D.; Proniewicz, L. M.; Fausto, R. Importance of Entropy in the Conformational Equilibrium of Phenylalanine: A Matrix-Isolation Infrared Spectroscopy and Density Functional Theory Study. *J. Phys. Chem. A* **2006**, *110*, 2360−2370.
(41) Ess, D. H.; Wheeler, S. E.; Iafe, R. G.; Xu, L.; Çelebi-Ölçüm, N.; Houk, K. N. Bifurcations on Potential Energy Surfaces of Organic Reactions. *Angew. Chem., Int. Ed.* **2008**, *47*, 7592−7601.
(42) Rehbein, J.; Carpenter, B. K. Do We Fully Understand What Controls Chemical Selectivity? *Phys. Chem. Chem. Phys.* **2011**, *13*, 20906−20922.
(43) Schreiner, P. R.; Reisenauer, H. P.; Ley, D.; Gerbig, D.; Wu, C.-H.; Allen, W. D. Methylhydroxycarbene: Tunneling Control of a Chemical Reaction. *Science* **2011**, *332*, 1300.
(44) Grimme, S.; Bohle, F.; Hansen, A.; Pracht, P.; Spicher, S.; Stahn, M. Efficient Quantum Chemical Calculation of Structure Ensembles and Free Energies for Nonrigid Molecules. *J. Phys. Chem. A* **2021**, *125*, 4039−4054.
(45) Pracht, P.; Bohle, F.; Grimme, S. Automated Exploration of the Low-Energy Chemical Space with Fast Quantum Chemical Methods. *Phys. Chem. Chem. Phys.* **2020**, *22*, 7169−7192.
(46) Car, R.; Parrinello, M. Unified Approach for Molecular Dynamics and Density-Functional Theory. *Phys. Rev. Lett.* **1985**, *55*, 2471−2474.
(47) Barnett, R. N.; Landman, U.; Nitzan, A.; Rajagopal, G. Born−Oppenheimer Dynamics Using Density-functional Theory: Equilibrium and Fragmentation of Small Sodium Clusters. *J. Chem. Phys.* **1991**, *94*, 608−616.
(48) Urakawa, A.; Iannuzzi, M.; Hutter, J.; Baiker, A. Towards a Rational Design of Ruthenium CO2 Hydrogenation Catalysts by Ab Initio Metadynamics. *Chem.—Eur. J.* **2007**, *13*, 6828−6840.
(49) Schilling, M.; Cunha, R. A.; Luber, S. Enhanced Ab Initio Molecular Dynamics Exploration Unveils the Complex Role of Different Intramolecular Bases on the Water Nucleophilic Attack Mechanism. *ACS Catal.* **2020**, *10*, 7657−7667.
(50) Adenusi, H.; Le Donne, A.; Porcelli, F.; Bodo, E. Ab Initio Molecular Dynamics Study of Phospho-Amino Acid-Based Ionic Liquids: Formation of Zwitterionic Anions in the Presence of Acidic Side Chains. *J. Phys. Chem. B* **2020**, *124*, 1955−1964.
(51) Bodo, E.; Bonomo, M.; Mariani, A. Assessing the Structure of Protic Ionic Liquids Based on Triethylammonium and Organic Acid Anions. *J. Phys. Chem. B* **2021**, *125*, 2781−2792.
(52) Karimova, N. V.; Alves, M. R.; Luo, M.; Grassian, V. H.; Gerber, R. B. Toward a Microscopic Model of Light Absorbing Dissolved Organic Compounds in Aqueous Environments: Theoretical and Experimental Study. *Phys. Chem. Chem. Phys.* **2021**, *23*, 10487−10497.
(53) Tran, T.; Prlj, A.; Lin, K.-H.; Hollas, D.; Corminboeuf, C. Mechanisms of Fluorescence Quenching in Prototypical Aggregation-Induced Emission Systems: Excited State Dynamics with TD-DFTB. *Phys. Chem. Chem. Phys.* **2019**, *21*, 9026−9035.
(54) Muždalo, A.; Saalfrank, P.; Vreede, J.; Santer, M. Cis-to-Trans Isomerization of Azobenzene Derivatives Studied with Transition Path Sampling and Quantum Mechanical/Molecular Mechanical Molecular Dynamics. *J. Chem. Theory Comput.* **2018**, *14*, 2042−2051.
(55) Sakti, A. W.; Nishimura, Y.; Nakai, H. Rigorous PKa Estimation of Amine Species Using Density-Functional Tight-Binding-Based Metadynamics Simulations. *J. Chem. Theory Comput.* **2018**, *14*, 351−356.
(56) Grimme, S. Exploration of Chemical Compound, Conformer, and Reaction Space with Meta-Dynamics Simulations Based on Tight-Binding Quantum Chemical Calculations. *J. Chem. Theory Comput.* **2019**, *15*, 2847−2862.
(57) Sauceda, H. E.; Vassilev-Galindo, V.; Chmiela, S.; Müller, K.-R.; Tkatchenko, A. Dynamical Strengthening of Covalent and Non-Covalent Molecular Interactions by Nuclear Quantum Effects at Finite Temperature. *Nat. Commun.* **2021**, *12*, 442.
(58) Lahey, S.-L. J.; Rowley, C. N. Simulating Protein−Ligand Binding with Neural Network Potentials. *Chem. Sci.* **2020**, *11*, 2362−2368.
(59) Cole, D. J.; Mones, L.; Csányi, G. A Machine Learning Based Intramolecular Potential for a Flexible Organic Molecule. *Faraday Discuss.* **2020**, *224*, 247−264.
(60) Chmiela, S.; Tkatchenko, A.; Sauceda, H. E.; Poltavsky, I.; Schütt, K. T.; Müller, K. R. Machine Learning of Accurate Energy-Conserving Molecular Force Fields. *Sci. Adv.* **2017**, *3*, No. e1603015.
(61) Behler, J.; Parrinello, M. Generalized Neural-Network Representation of High-Dimensional Potential-Energy Surfaces. *Phys. Rev. Lett.* **2007**, *98*, 146401.
(62) Bartók, A. P.; Payne, M. C.; Kondor, R.; Csányi, G. Gaussian Approximation Potentials: The Accuracy of Quantum Mechanics, without the Electrons. *Phys. Rev. Lett.* **2010**, *104*, 136403.
(63) Bartók, A. P.; De, S.; Poelking, C.; Bernstein, N.; Kermode, J. R.; Csányi, G.; Ceriotti, M. Machine Learning Unifies the Modeling of Materials and Molecules. *Sci. Adv.* **2017**, *3*, No. e1701816.
(64) Petraglia, R.; Nicolaï, A.; Wodrich, M. D.; Ceriotti, M.; Corminboeuf, C. Beyond Static Structures: Putting Forth REMD as a Tool to Solve Problems in Computational Organic Chemistry. *J. Comput. Chem.* **2016**, *37*, 83−92.

https://doi.org/10.1021/acs.joc.1c02991
J. Org. Chem. 2022, 87, 8849−8857

(65) Rossi, K.; Jurásková, V.; Wischert, R.; Garel, L.; Corminbœuf, C.; Ceriotti, M. Simulating Solvation and Acidity in Complex Mixtures with First-Principles Accuracy: The Case of CH_3SO_3H and H_2O_2 in Phenol. *J. Chem. Theory Comput.* **2020**, *16*, 5139−5149.
(66) Fabregat, R.; Fabrizio, A.; Meyer, B.; Hollas, D.; Corminboeuf, C. Hamiltonian-Reservoir Replica Exchange and Machine Learning Potentials for Computational Organic Chemistry. *J. Chem. Theory Comput.* **2020**, *16*, 3084−3094.
(67) Dijkstra, G. D. H.; Kellogg, R. M.; Wynberg, H.; Svendsen, J. S.; Marko, I.; Sharpless, K. B. Conformational Study of Cinchona Alkaloids. A Combined NMR, Molecular Mechanics and x-Ray Approach. *J. Am. Chem. Soc.* **1989**, *111*, 8069−8076.
(68) Zhou, J.; Wakchaure, V.; Kraft, P.; List, B. Primary-Amine-Catalyzed Enantioselective Intramolecular Aldolizations. *Angew. Chem., Int. Ed.* **2008**, *47*, 7656−7658.
(69) Pérez-Estrada, S.; Rodrıguez-Molina, B.; Xiao, L.; Santillan, R.; Jiménez-Osés, G.; Houk, K. N.; Garcia-Garibay, M. A. Thermodynamic Evaluation of Aromatic CH/π Interactions and Rotational Entropy in a Molecular Rotor. *J. Am. Chem. Soc.* **2015**, *137*, 2175−2178.
(70) Sugita, Y.; Okamoto, Y. Replica-Exchange Molecular Dynamics Method for Protein Folding. *Chem. Phys. Lett.* **1999**, *314*, 141−151.
(71) Gaus, M.; Cui, Q.; Elstner, M. DFTB3: Extension of the Self-Consistent-Charge Density-Functional Tight-Binding Method (SCC-DFTB). *J. Chem. Theory Comput.* **2011**, *7*, 931−948.
(72) Gaus, M.; Goez, A.; Elstner, M. Parametrization and Benchmark of DFTB3 for Organic Molecules. *J. Chem. Theory Comput.* **2013**, *9*, 338−354.
(73) Gaus, M.; Lu, X.; Elstner, M.; Cui, Q. Parameterization of DFTB3/3OB for Sulfur and Phosphorus for Chemical and Biological Applications. *J. Chem. Theory Comput.* **2014**, *10*, 1518−1537.
(74) Peters, M. V.; Stoll, R. S.; Kühn, A.; Hecht, S. Photoswitching of Basicity. *Angew. Chem., Int. Ed.* **2008**, *47*, 5968−5972.
(75) Stoll, R. S.; Peters, M. V.; Kuhn, A.; Heiles, S.; Goddard, R.; Bühl, M.; Thiele, C. M.; Hecht, S. Photoswitchable Catalysts: Correlating Structure and Conformational Dynamics with Reactivity by a Combined Experimental and Computational Approach. *J. Am. Chem. Soc.* **2009**, *131*, 357−367.
(76) Stoll, R. S.; Hecht, S. Immobilization of a Photoswitchable Piperidine Base. *Org. Lett.* **2009**, *11*, 4790−4793.
(77) Pescher, M. D.; van Wilderen, L. J. G. W.; Grützner, S.; Slavov, C.; Wachtveitl, J.; Hecht, S.; Bredenbeck, J. Ultrafast Light-Driven Substrate Expulsion from the Active Site of a Photoswitchable Catalyst. *Angew. Chem., Int. Ed.* **2017**, *56*, 12092−12096.
(78) Henry, L. *C. R. Hebd. Seances Acad. Sci.* **1895**, *120*, 1265−1268.
(79) Luzzio, F. A. The Henry Reaction: Recent Examples. *Tetrahedron* **2001**, *57*, 915−945.
(80) Grimme, S.; Ehrlich, S.; Goerigk, L. Effect of the Damping Function in Dispersion Corrected Density Functional Theory. *J. Comput. Chem.* **2011**, *32*, 1456−1465.
(81) Aradi, B.; Hourahine, B.; Frauenheim, T. DFTB+, a Sparse Matrix-Based Implementation of the DFTB Method. *J. Phys. Chem. A* **2007**, *111*, 5678−5684.
(82) Frisch, M. J.; Trucks, G. W.; Schlegel, H. B.; Scuseria, G. E.; Robb, M. A.; Cheeseman, J. R.; Scalmani, G.; Barone, V.; Petersson, G. A.; Nakatsuji, H.; Li, X.; Caricato, M.; Marenich, A. V.; Bloino, J.; Janesko, B. G.; Gomperts, R.; Mennucci, B.; Hratchian, H. P.; Ortiz, J. V.; Izmaylov, A. F.; Sonnenberg, J. L.; Williams-Young, D.; Ding, F.; Lipparini, F.; Egidi, F.; Goings, J.; Peng, B.; Petrone, A.; Henderson, T.; Ranasinghe, D.; Zakrzewski, V. G.; Gao, J.; Rega, N.; Zheng, G.; Liang, W.; Hada, M.; Ehara, M.; Toyota, K.; Fukuda, R.; Hasegawa, J.; Ishida, M.; Nakajima, T.; Honda, Y.; Kitao, O.; Nakai, H.; Vreven, T.; Throssell, K.; Montgomery, J. A., Jr.; Peralta, J. E.; Ogliaro, F.; Bearpark, M. J.; Heyd, J. J.; Brothers, E. N.; Kudin, K. N.; Staroverov, V. N.; Keith, T. A.; Kobayashi, R.; Normand, J.; Raghavachari, K.; Rendell, A. P.; Burant, J. C.; Iyengar, S. S.; Tomasi, J.; Cossi, M.; Millam, J. M.; Klene, M.; Adamo, C.; Cammi, R.; Ochterski, J. W.; Martin, R. L.; Morokuma, K.; Farkas, O.; Foresman, J. B.; Fox, D. J. *Gaussian 16*, Revision C.01; Gaussian, Inc.: Wallingford CT, 2016.
(83) Rüger, R.; Franchini, M.; Trnka, T.; Yakovlev, A.; van Lenthe, E.; Philipsen, P.; van Vuren, T.; Klumpers, B.; Soini, T. *AMS, SCM, Theoretical Chemistry*; Vrije Universiteit: Amsterdam, The Netherlands, 2021.
(84) te Velde, G.; Bickelhaupt, F. M.; Baerends, E. J.; Fonseca Guerra, C.; van Gisbergen, S. J. A.; Snijders, J. G.; Ziegler, T. Chemistry with ADF. *J. Comput. Chem.* **2001**, *22*, 931−967.
(85) Ceriotti, M.; More, J.; Manolopoulos, D. E. i-PI: A Python Interface for Ab Initio Path Integral Molecular Dynamics Simulations. *Comput. Phys. Commun.* **2014**, *185*, 1019−1026.
(86) Bonomi, M.; Branduardi, D.; Bussi, G.; Camilloni, C.; Provasi, D.; Raiteri, P.; Donadio, D.; Marinelli, F.; Pietrucci, F.; Broglia, R. A.; Parrinello, M. PLUMED: A Portable Plugin for Free-Energy Calculations with Molecular Dynamics. *Comput. Phys. Commun.* **2009**, *180*, 1961−1972.
(87) Tribello, G. A.; Bonomi, M.; Branduardi, D.; Camilloni, C.; Bussi, G. PLUMED 2: New Feathers for an Old Bird. *Comput. Phys. Commun.* **2014**, *185*, 604−613.
(88) Bonomi, M.; Bussi, G.; Camilloni, C.; Tribello, G. A.; Banáš, P.; Barducci, A.; Bernetti, M.; Bolhuis, P. G.; Bottaro, S.; Branduardi, D.; Capelli, R.; Carloni, P.; Ceriotti, M.; Cesari, A.; Chen, H.; Chen, W.; Colizzi, F.; De, S.; De La Pierre, M.; Donadio, D.; Drobot, V.; Ensing, B.; Ferguson, A. L.; Filizola, M.; Fraser, J. S.; Fu, H.; Gasparotto, P.; Gervasio, F. L.; Giberti, F.; Gil-Ley, A.; Giorgino, T.; Heller, G. T.; Hocky, G. M.; Iannuzzi, M.; Invernizzi, M.; Jelfs, K. E.; Jussupow, A.; Kirilin, E.; Laio, A.; Limongelli, V.; Lindorff-Larsen, K.; Löhr, T.; Marinelli, F.; Martin-Samos, L.; Masetti, M.; Meyer, R.; Michaelides, A.; Molteni, C.; Morishita, T.; Nava, M.; Paissoni, C.; Papaleo, E.; Parrinello, M.; Pfaendtner, J.; Piaggi, P.; Piccini, G.; Pietropaolo, A.; Pietrucci, F.; Pipolo, S.; Provasi, D.; Quigley, D.; Raiteri, P.; Raniolo, S.; Rydzewski, J.; Salvalaglio, M.; Sosso, G. C.; Spiwok, V.; Šponer, J.; Swenson, D. W. H.; Tiwary, P.; Valsson, O.; Vendruscolo, M.; Voth, G. A.; White, A. Promoting Transparency and Reproducibility in Enhanced Molecular Simulations. *Nat. Methods* **2019**, *16*, 670−673.
(89) Huang, M.; Dissanayake, T.; Kuechler, E.; Radak, B. K.; Lee, T.-S.; Giese, T. J.; York, D. M. A Multidimensional B-Spline Correction for Accurate Modeling Sugar Puckering in QM/MM Simulations. *J. Chem. Theory Comput.* **2017**, *13*, 3975−3984.
(90) Gruden, M.; Andjeković, L.; Jissy, A. K.; Stepanović, S.; Zlatar, M.; Cui, Q.; Elstner, M. Benchmarking Density Functional Tight Binding Models for Barrier Heights and Reaction Energetics of Organic Molecules. *J. Comput. Chem.* **2017**, *38*, 2171−2185.
(91) Note that the value d = 4.2 Å used to discriminate between ON and OFF states was chosen based on the comparison between the distribution histograms of all the conformers of the (E)- and (Z)-configurations sampled (see the Supporting Information).
(92) Anslyn, E. V.; Dougherty, D. A. Strain and Stability - Relationships Between Structure and Energetics−Basic Conformational Analysis. *Modern Physical Organic Chemistry*; University Science Books, 2006; p 104.
(93) Zhao, Y. H.; Abraham, M. H.; Zissimos, A. M. Fast Calculation of van Der Waals Volume as a Sum of Atomic and Bond Contributions and Its Application to Drug Compounds. *J. Org. Chem.* **2003**, *68*, 7368−7373.
(94) Liu, P.; Kim, B.; Friesner, R. A.; Berne, B. J. Replica Exchange with Solute Tempering: A Method for Sampling Biological Systems in Explicit Water. *Proc. Natl. Acad. Sci. U.S.A.* **2005**, *102*, 13749−13754.
(95) Jurásková, V.; Célerse, F.; Laplaza, R.; Corminboeuf, C. Assessing the persistence of chalcogen bonds in solution with neural network potentials. *J. Chem. Phys.* **2022**, *156*, 154112.

https://doi.org/10.1021/acs.joc.1c02991
J. Org. Chem. 2022, 87, 8849−8857